Ultrasound in Med. & Biol., Vol. 45, No. 11, pp. 3028–3041, 2019

0301-5629/$ - see front matter

https://doi.org/10.1016/j.ultrasmedbio.2019.07.683

● *Original Contribution*

EFFECT OF ULTRASOUND ON THE VASCULATURE AND EXTRAVASATION OF NANOSCALE PARTICLES IMAGED IN REAL TIME

Petros T. Yemane,* Andreas K.O. Åslund,*,†,‡ Sofie Snipstad,*,†,§ Astrid Bjørkøy,* Kristin Grendstad,* Sigrid Berg,§,¶,‖ Yrr Mørch,† Sverre H. Torp,#,** Rune Hansen,¶,‖ and Catharina de Lange Davies*

* Department of Physics, Norwegian University of Science and Technology, Trondheim, Norway; † Department of Biotechnology and Nanomedicine, SINTEF Industry, Trondheim, Norway; ‡ Stroke Unit, Department of Internal Medicine, St. Olav's Hospital, Trondheim, Norway; § Cancer Clinic, St. Olav's Hospital, Trondheim, Norway; ¶ Department of Circulation and Medical Imaging, Norwegian University of Science and Technology, Trondheim, Norway; ‖ Department of Health Research, SINTEF Digital, Trondheim, Norway; # Department of Pathology, St. Olav's Hospital, Trondheim, Norway; and ** Department of Clinical and Molecular Medicine, Norwegian University of Science and Technology, Trondheim, Norway

(*Received* 3 *June* 2019; *revised* 31 *July* 2019; *in final from* 31 *July* 2019)

Abstract—Ultrasound and microbubbles have been found to improve the delivery of drugs and nanoparticles to tumor tissue. To obtain new knowledge on the influence of vascular parameters on extravasation and to elucidate the effect of acoustic pressure on extravasation and penetration of nanoscale particles into the extracellular matrix, real-time intravital multiphoton microscopy was performed during sonication of tumors growing in dorsal window chambers. The impact of vessel diameter, vessel structure and blood flow was characterized. Fluorescein isothiocyanate–dextran (2 MDa) was injected to visualize blood vessels. Mechanical indexes (MI) of 0.2–0.8 and in-house-made, nanoparticle-stabilized microbubbles or Sonovue were applied. The rate and extent of penetration into the extracellular matrix increased with increasing MI. However, to achieve extravasation, smaller vessels required MIs (0.8) higher than those of blood vessels with larger diameters. Ultrasound changed the blood flow rate and direction. Interestingly, the majority of extravasations occurred at vessel branching points. (E-mail: Catharina.davies@ntnu.no)

Key Words: **Ultrasound, Microbubbles, Real-time imaging, Multiphoton microscope, Cavitation, Blood flow, Vascular structure, Nanoparticle delivery.**

INTRODUCTION

Intravenous delivery of therapeutic agents to tumors in patients in optimal quantities with limited exposure to normal tissue is challenging (Tannock et al. 2002). The administered drugs cause severe side effects because of their accumulation in healthy tissue (Coates et al. 1983). Encapsulating therapeutic drugs into nanoparticles (NPs) might enhance the tumor uptake of drugs and reduce the toxic effects on healthy tissue through the enhanced permeability and retention effect (Maeda et al. 2000). However, an improved therapeutic response has not been reported in the clinic (Lammers et al. 2012). A recent meta-analysis of pre-clinical studies in the last 10 y found that only 0.7% of the injected NPs accumulated in tumors (Wilhelm et al. 2016). The primary reason for this finding is that the NPs must pass several physiologic barriers before reaching the diseased cells (Anchordoquy et al. 2017; Mullick Chowdhury et al. 2017; Wang et al. 2014a).

The distribution of NPs in tumors is notably heterogeneous, and NPs are mainly located close to the capillary wall (Boissenot et al. 2016; Eggen et al. 2014; Lammers et al. 2012). Thus, a more efficient method for delivering therapeutic agents is needed.

Focused ultrasound (FUS) and systemic administration of microbubbles (MBs) have been reported to improve the delivery and therapeutic response of drugs

Address correspondence to: Catharina de Lange Davies, Department of Physics, Norwegian University of Science and Technology, Høgskoleringen 5, 7491 Trondheim Norway. E-mail: Catharina.davies@ntnu.no

and NPs in pre-clinical studies (Kotopoulis et al. 2014; Lammertink et al. 2015; Snipstad et al. 2017; Treat et al. 2012; van Wamel et al. 2016). A clinical study in which patients with non-resectable pancreatic tumors were treated with gemcitabine combined with FUS and MBs reported improved therapeutic response in a subgroup of patients (Dimcevski et al. 2016). FUS and MBs have also been found to open the blood–brain barrier, both in pre-clinical studies (Åslund et al. 2015; Hynynen et al. 2001; Liu et al. 2010; Nhan et al. 2013; Wei et al. 2013) and in humans (Carpentier et al. 2016; Mainprize et al. 2019).

The exact mechanisms underlying FUS- and MB-mediated drug delivery have not been thoroughly elucidated to date. Ultrasound (US)-induced bio-effects can be divided into thermal and non-thermal effects. The thermal effect is generally not considered to play a major role in microbubble-assisted treatments at relatively low mechanical indexes (MIs). The non-thermal effects are due to mechanical effects through acoustic radiation force and cavitation which is considered to be the most important mechanism for therapeutic applications when US is used in combination with MBs (Hernot and Klibanov 2008). The acoustic radiation force is the transfer of momentum from the US wave, which causes the translation of particles (Antonios and James 2016) and MBs (Dayton et al. 1999) in the direction of US wave propagation. Cavitation is the formation and volumetric oscillation of MBs in response to the pressure amplitude of the US wave. A stable volumetric oscillation of MBs at equilibrium radius for many acoustic cycles is called *stable cavitation*, whereas a large and unstable expansion of the bubble during the acoustic wave at higher pressures, which results in violent collapse, is known as *inertial cavitation*.

Cavitation in a medium depends strongly on the acoustic parameters and the presence and size of MBs. Acoustic parameters such as pressure and frequency can alter the MB response from stable cavitation to inertial cavitation. It has been reported that pulse duration is also highly important for the onset of the stable and inertial cavitation of MBs (Wang et al. 2015). In addition, MB concentration and size will significantly affect cavitation activity (McMahon and Hynynen 2017; Wang et al. 2014b). In addition, the space available for the MBs to oscillate and the proximity to the vessel wall are of great importance for the effect of cavitation on the vessel wall and, thus, the outcome of US-mediated drug delivery (Garbin et al. 2007; Helfield et al. 2014).

Cavitation-induced bio-effects caused by MBs oscillating close to the vessel wall include acoustic microstreaming, shock waves and microjetting, the latter caused by the violent collapse of bubbles; all create temporary and/or permanent gaps in the blood vessel walls (Chen et al. 2010, 2011). Cavitation-induced mechanical force that can distend and invaginate the vessel wall could also enhance vascular permeability (Caskey et al. 2007; Chen et al. 2011). These cavitation-induced bio-effects can also create unwanted and unintended permanent damage to the blood vessel. However, cavitation can be exploited for drug delivery if the US parameters are well optimized.

To understand in more detail how US and MBs enhance the permeability of biological barriers, direct observation of the behavior of the bubbles in real time is necessary (Caskey et al. 2007; Chen et al. 2011; Helfield et al. 2016; Raymond et al. 2007). Thus, tumors were grown in dorsal window chambers, which enabled us to simultaneously apply US and image the vasculature by intravital multiphoton microscopy. We compared two different MBs: in-house-made MBs stabilized by polymeric NPs (NPMBs) (Mørch et al. 2015) and Sonovue co-administered with the same polymeric NPs during FUS. NPs were administered with Sonovue to compare the efficacy of the two MBs on the extravasation of the NPs. Because the fluorescence from the NPs is not homogenous enough to delineate the blood vessels, dextran (2 MDa) was injected to visualize the blood vessel and to study the extravasation of the dextran. The aim was to reveal vascular parameters as well as NP and MB behavior influencing extravasation and the effect of different MIs on extravasation and penetration of NPs into the extracellular matrix. In particular, we imaged whether the blood flow, the vascular structure and the size of the vessel influenced where extravasations could be detected. Moreover, histologic examination of paraffin sections of the tissue was performed to evaluate tissue damage.

METHODS

Cell culture

A human osteosarcoma cell line (OHS) was used (Fodstad et al. 1986). Cells were grown in Roswell Park Memorial Institute-1640 medium (Gibco Thermo-Fisher, 21875-034, Oslo, Norway) supplemented with 10% fetal bovine serum (Sigma-Aldrich, Oslo, Norway), 100 U/mL penicillin and 100 μg/mL streptomycin (Sigma-Aldrich) at 37°C and 5% CO_2.

Animal model and dorsal window chamber implantation

A previous study had found that OHS tumors are well vascularized throughout the tumor and have no necrotic core (Sulheim et al. 2018). The OHS tumors were grown as xenografts in male BALB/c nude mice (weight: 23–30 g, Janvier, Le Genest-Saint-Isle, France) in dorsal skinfold window chambers (Fig. 1a).

Dorsal skinfold window chamber surgery was carried out as previously described by Hak et al. (2010). Briefly, the double layer of the skin was sandwiched between two symmetric frames, and a circular area

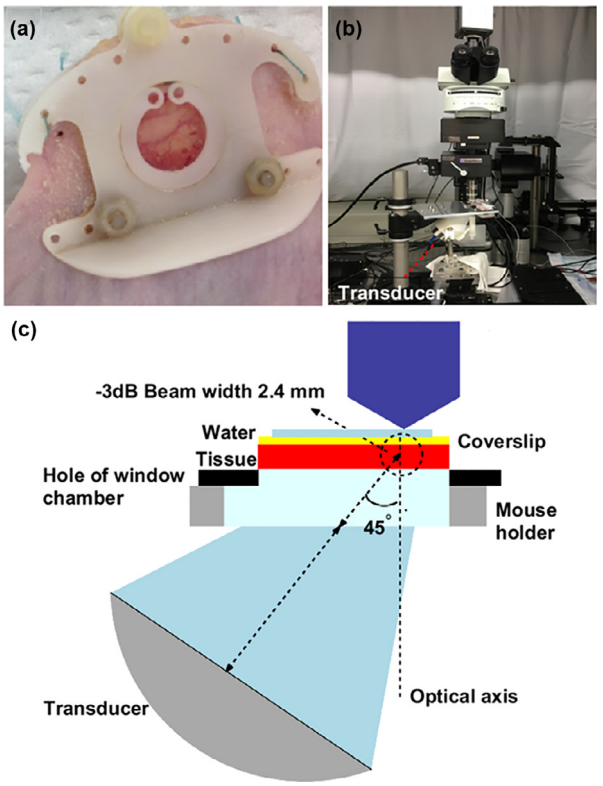

Fig. 1. Schematic of the US and multiphoton microscope setup for US−microbubble-mediated drug delivery in a skin flap dorsal window chamber. (a) Dorsal window chamber. (b) Experimental setup. (c) US and objective/light beam alignment (not drawn to scale). US = ultrasound.

15 mm in diameter was removed from the skin on one side of the fold. The remaining layers of the other skinfold (thin striated skin muscle, subcutaneous tissue, dermis and epidermis) were covered with a glass coverslip, which was incorporated into one of the chamber frames and formed a window to the tissue. The next day, 30 μL containing 5×10^6 OHS cells were implanted in the window chamber. Tumors were grown for 2 wk before treatment. The tumor thickness was limited by the window chamber, while the diameter in the longest direction was typically 5−10 mm. The animals tolerated the chambers well and exhibited no signs of discomfort. The water for the animals was supplemented with 25 mg/mL Baytril (Bayer, Oslo, Norway), and they were kept in separate cages after the window chamber was implanted. All surgical and imaging procedures were performed with the animal anesthetized by a subcutaneous injection of fentanyl (0.05 mg/kg, Actavis Group HF)/medetomidine (0.5 mg/kg, Orion Pharma)/midazolam (5 mg/kg Accord Healthcare Limited)/water (2:1:2:5) at a dose of 0.1 mL per 10 g weight. All animal experiments were approved by the Norwegian Animal Research Authorities, that is, the Norwegian Food Safety Authority.

Nanoparticles and microbubbles

In-house self-assembled NP-stabilized MBs (mean diameter of 2.4 ±0.2 μm, SINTEF, Trondheim, Norway) and the commercial phospholipid-shelled Sonovue (mean diameter = 2.5 μm, Bracco, Milan, Italy) were used. The size distribution of the two MB types is illustrated in Supplementary Figure S1 (online only). Briefly, poly(2-ethylbutyl cyanoacrylate) [PEBCA] NPs were synthesized by mini-emulsion polymerization and contained the dye NR668 (2%, modified Nile Red, custom synthesis) (Klymchenko et al. 2012; Mørch et al. 2015), which possess excitation and emission maxima of 548 and 621 nm, respectively. The PEBCA NPs were used to make NPMBs by mixing casein and perfluoropropane gas using an Ultra-Turrax at 24,000 rpm for 4 min. The resulting NPMB solution contained an excess of free NPs.

Before each sonication, 30 μL (4 mg/mL, diluted in saline) of 2 MDa fluorescein isothiocyanate (FITC)−dextran (Sigma-Aldrich) was injected through the tail vein to visualize the blood vessels. Mice in the NPMB groups were given a bolus injection of 50 μL of NPMBs ($2-5 \times 10^8$ MBs/mL, 10 mg/mL NPs), whereas mice in the Sonovue groups received 25 μL (20 mg/mL, diluted in 0.01 M phosphate buffer) of free PEBCA NPs before injection of 50 μL of Sonovue ($2-5 \times 10^8$ MBs/mL).

Ultrasound exposure setup

An experimental setup that enabled the application of US while imaging the dorsal window chamber with multiphoton microscopy was established. Figure 1 (b, c) is a schematic of the experimental setup. The US beam (at the region of interest [ROI]) was aligned with the focus of the objective using a custom-built 3D printed cone and calibrated fiberoptic hydrophone system (Precision Acoustics Ltd, Dorchester, UK) by monitoring the output pressure on an oscilloscope (TDS 210, Tektronix, Bracknell, UK). The cone was manufactured with inner diameters at top and bottom of 15 and 68 mm, respectively, and a cone length of 74 mm. The transducer was mounted on the bottom of the cone, and the cone was filled with distilled and degassed water. The axis of the US beam was 45° with respect to the imaging plane to minimize reflections from the glass of the window chamber and reduce standing wave formation. An ultrasonic coupling gel filled the gap between the tip of the cone and the skin of the mice.

Ultrasound parameters

A single-element focused transducer (Precision Acoustics Ltd,) with a 1-MHz center frequency, 60-mm diameter and 75-mm curvature was used. US pulses were generated by an arbitrary waveform generator (AWFG, 33522 A, Agilent Technologies, Santa Clara, CA, USA) and amplified by a 50-dB power amplifier

Table 1. Overview of the treated groups and number of observed extravasations

Group	NPMBs					Sonovue	
MI	0.2	0.4	0.6*	0.8	0.2†	0.4	0.8
Number of animals with PRF = 0.5 Hz (0.1 Hz)	5 (1)	5 (4)	3 (0)	9 (1)	4 (0)	6 (2)	5 (4)
Total number of treatments with PRF = 0.5 Hz (0.1 Hz)	7 (2)	9 (8)	6 (0)	15 (1)	4 (0)	9 (4)	9 (8)
Percentage of treatments in which extravasation occurred within the five regions imaged per total number of treatments with PRF = 0.5 Hz (0.1 Hz)	14% (100%)	56% (38%)	33% (0%)	73% (100%)	0%	22% (100%)	44% (88%)
Percentage of treatments in which extravasations were observed live during treatment per total number of treatments with PRF = 0.5 Hz (0.1 Hz)	14% (100%)	11% (38%)	17% (0%)	40% (100%)	0%	11% (50%)	0% (63%)
Total number of extravasations within the five regions imaged with PRF = 0.5 Hz (0.1 Hz)‡	2 (10)	5 (17)	5 (0)	45 (2)	0	10 (6)	9 (20)
Total number of extravasations observed during live imaging with PRF = 0.5 Hz (0.1 Hz)‡	2 (3)	1 (7)	3 (0)	15 (2)	0	2 (3)	0 (10)

MI = mechanical index; NPMBs = in-house-made MBs stabilized by polymeric nanoparticles; PRF = pulse repetition frequency.
Note: Some animals were treated at two MIs (low and high) at one position if no extravasation was observed at the lower MI.
* Few animals were treated and exhibited only three extravasations during live imaging at an MI of 0.6 combined with NPMBs (data are used only for analysis of vessel diameter and time of extravasation).
† Few animals were treated at a MI of 0.2, and no extravasation was observed during live imaging.
‡ In one treatment, multiple extravasations occurred.

(2100 L amplifier, ENI, USA). The transducer was characterized in a water tank measurement system (AIMS-III, Onda Corp.), and the pressure and −3-dB beam width at the ROI were measured with a calibrated HGL-0200 hydrophone (Onda Corp.) using an AH-2010 preamplifier (Onda Corp.). The −3-dB beam width at the target was 2.4 mm. The transducer was characterized both with and without the cone, and no differences in beam profile or pressure were found.

The tumor was sonicated with US pulses with a center frequency of 1 MHz, pulse length of 10 ms and pulse repetition frequency (PRF) of 0.5 or 0.1 Hz to allow MBs to reperfuse into the treatment area in the time between transmit pulses. The total duration of sonication was 5 min and was chosen based on the circulation half-life of the MBs. The circulation half-time of NPMBs is approximately 1.5−2 times longer than for Sonovue, which is 1 min (Schneider 1999; Wu et al. 2017). Peak negative pressure amplitudes of 0.2, 0.4, 0.6 and 0.8 MPa, which were measured in water, were applied.

Treatment groups and controls

An overview of the different treatment groups and the number of mice treated is provided in Table 1. In total, 36 mice (18 mice each for the NPMB and Sonovue groups) were used. Eight mice (5 for the NPMB group and 3 for the Sonovue group) received two different MIs (low MI [0.2 and 0.4] and high MI [0.6 and 0.8]) at the same position, and each mouse was treated in two different positions (Fig. 2b). Thus, in Table 1, a single mouse is counted in multiple different MI groups in some cases. Every mouse received US, and pre-images were recorded as control before US was applied for every treatment (Fig. 2a). To study blood flow and possible extravasation before US and MB injection, mice (n = 16) received an intravenous injection of FITC−dextran and were imaged for 3−5 min. Subsequently, NPMBs (n = 4) or NPs and Sonovue (n = 3) were injected, and the tumor was imaged at the same field of view (FOV) for an additional 5 min before sonication. The remaining mice (n = 9) received US immediately after NPs and MBs were injected; that is,

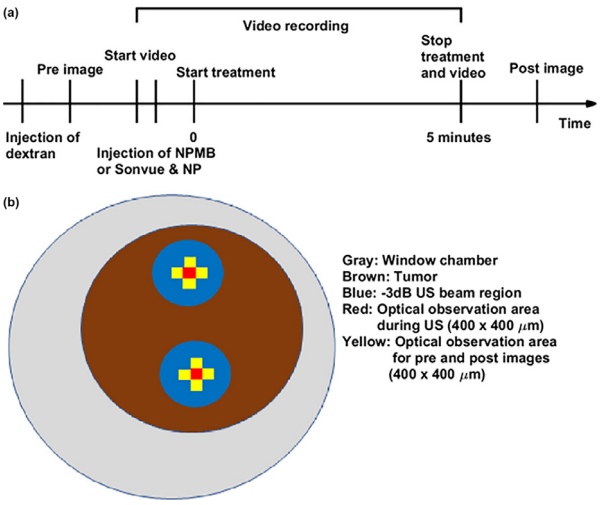

Fig. 2. (a) Treatment and imaging schedule. (b) Two treatment areas and imaging areas where images were acquired before, during and after US. After 2-MDa fluorescein isothiocyanate−dextran was injected, multiphoton pre-images were acquired (*yellow*), video recording started (*red*) and NPMBs or Sonovue MB and NPs were injected before sonication started (*blue*). After US, post-images were acquired. MB = microbubbles; NP = nanoparticles; NPMB = nanoparticle-stabilized microbubbles; US = ultrasound.

the effects of NPs and MBs on blood flow and extravasation were not imaged before US exposure.

Real-time multiphoton microscope imaging during ultrasound exposure

Mice with dorsal window chambers were anesthetized and positioned on a custom-designed microscope stage with a heating device maintaining the body temperature at 37°C, as illustrated in Figure 1. The tail vein was cannulated for intravenous administration. The treatment and imaging schedule are illustrated in Figure 2a.

The multiphoton microscope (*in vivo* SliceScope, Scientifica, Uckfield, UK) was equipped with a 20 × water dipping objective (XLUMPLFLN20 XW from Olympus, numerical aperture (NA) = 1.0 working distance 2 mm) and a pulsed MaiTai DeepSee (Spectra-Physics, Mountain View CA, USA) laser. The excitation wavelength was 790 nm. Images were acquired in resonant scanning mode at 31 frames per second (fps; 512 × 512 pixels) with a FOV of 400 × 400 μm. The filters in front of the two GaAsp detectors were long pass 590 nm and bandpass 525/50 nm for the detection of NPs with NR668 and FITC−dextran, respectively.

After pre-images of the vessels were acquired at the five neighboring positions (one red and four yellow) illustrated in Figure 2b, video-rate imaging started at the red area immediately before NPMBs or Sonovue and NPs were injected. US exposure started immediately after injection of the MBs. The video was recorded during the 5-min sonication.

After sonication, images were immediately recorded in the four yellow areas to observe any change during US exposure. Because the diameter of the tumor and the −3-dB US beam width are 5−10 and 2.4 mm, respectively, US exposure was performed in two different areas in each window chamber (Fig. 2b).

Histologic evaluation

All mice were euthanized by cervical dislocation. The tumor tissue was harvested and fixed in 4% buffered formaldehyde and embedded in paraffin. Finally, 5-μm-thick sections of the tissues from three different depths separated by 100 μm were prepared. The tissue was stained with hematoxylin, erythrosine and saffron (HES) to evaluate tissue damage after US treatment. A pathologist blinded to the study evaluated the tissue sections.

Image analysis

Images were analyzed using ImageJ (National Institutes of Health, Bethesda, MD, USA) and MATLAB (The MathWorks, Natick, MA, USA). To enhance the quality of the images, video frame averaging of several consecutive images was performed in ImageJ, as explained below. Then, the images were loaded into MATLAB. First, the images were median filtered (3 × 3 neighborhood) and segmented automatically.

Vascular masks (Supplementary Fig. S2, online only) were created using the first frame of the video of the FITC−dextran signal. In videos where extensive extravasation of NPs and dextran was observed, three consecutive images were averaged (compromise between the quality of the image and the time resolution). Then, a circle with the radius of the blood vessel and concentric circles spaced by 3 pixels (2.23 μm) starting from the center of the blood vessel were drawn. The normalized signal intensity (with respect to the maximum intensity in the whole image) of NPs and dextran within the blood vessel and in the different annuli over both time and distance were computed with the background subtracted. Then, the penetration of the NPs and dextran was estimated. Moreover, intravascular and extravascular accumulation (from the blood vessel wall until 50 μm into the extracellular matrix) of average fluorescence intensities of NPs and dextran were determined with the background subtracted. During extravascular analysis, video frame averaging of 15 consecutive images was performed. Some vessels were excluded from analysis of extravasation and penetration of the dextran and NPs if the source of the extravasation was uncertain. In addition, the average diameter of the blood vessel where extravasation was observed was computed from the pre-images (from both the *red* and *yellow* regions in Fig. 2b). The speed of NPs was estimated by tracking the distance NPs moved inside the vessels between subsequent frames. From 60 to 80 NPs were analyzed for each group. The occurrence of change in blood flow direction was determined by visual observations both before and during US. Any change in flow direction observed during the live imaging was counted as one occurrence; in other words, the total number of changes in blood flow direction is not given. The change in the flux of dextran in the blood vessels before and during US was estimated by measuring the intensity of FITC−dextran in a circular ROI drawn in blood vessels. A supplement is provided for detailed description of the method and some supplementary results (online only).

Statistical analysis

Data are presented as the mean value ± standard deviation. Analysis of variance was used for comparisons of differences between treatment groups in a confirmatory test. The Tukey−Kramer test (p value ≤ 0.05) was used to determine which pairwise comparisons were significant.

RESULTS

The effect of US combined with MBs on the extravasation of 2-MDa dextran and NPs was imaged in real time by intravital multiphoton microscopy during US sonication.

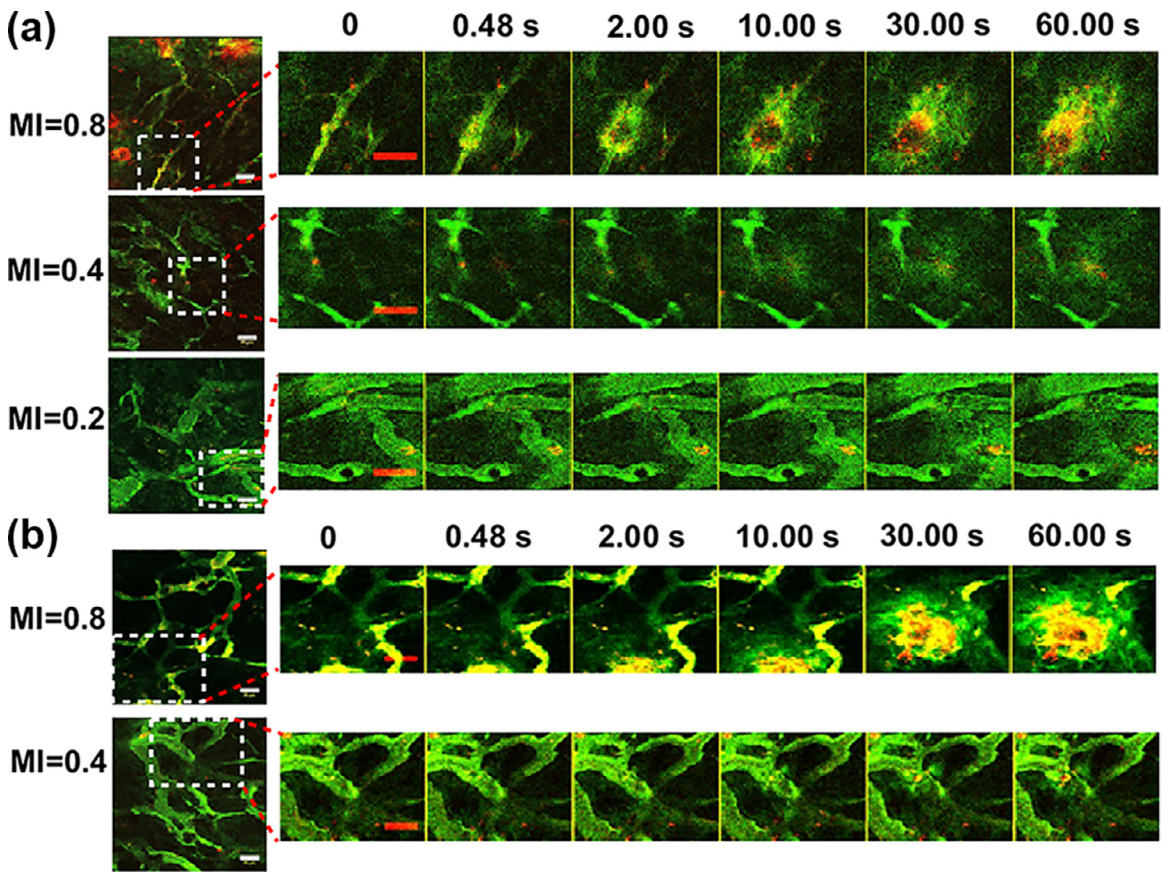

Fig. 3. Examples of extravasation and distribution of nanoparticles (*red*) and dextran (*green*) as a function of time after opening of the blood vessel wall by ultrasound and microbubbles with (a) nanoparticle-stabilized microbubbles at MIs of 0.8, 0.4 and 0.2 and (b) Sonovue at MIs of 0.8 and 0.4. Zero time corresponds to the time immediately before the extravasation event occurred. Bar = 50 μm. MI = mechanical index.

We observed extravasation and penetration of dextran and NPs into the extracellular matrix at all MIs tested and found a correlation between blood vessel diameter at which extravasation of NPs and dextran occurred and MI. Changes in flow rate and flow direction were observed, and occasionally, the blood flow stopped for short periods.

US-Induced extravasation of 2-MDa dextran and NPs

Representative images of extravasation of NPs (*red*) and dextran (*green*) from the blood vessel into the extracellular matrix as a function of time are shown in Figure 3, Supplementary Figure S3 (online only) and Supplementary Videos S1−S5 (online only). Extravasation of NPs and dextran was observed after sonication at MIs of 0.8, 0.4 and 0.2 when injecting NPMBs (Fig. 3a) and at MIs of 0.8 and 0.4 when injecting Sonovue (Fig. 3b). No extravasation of NPs and dextran was observed using an MI of 0.2 after administration of Sonovue. Because the NPMB solution also contains free NPs, the red signal observed in the videos could be NPMBs, free NPs or aggregated NPs.

The number and percentage of extravasation events (both NPs and dextran) per total number of treatments are given in Table 1. Both the number of extravasations in the FOV during US imaging and the number of extravasations counted in the five areas imaged after treatment are presented. Comparison of the two MBs reveals that the percentage of extravasation occurrence per total number of treatments at a PRF of 0.5 is higher for NPMBs than Sonovue at MIs of 0.8 (73% vs. 44%) and 0.4 (56% vs. 22%). After use of a lower PRF at 0.1 Hz, the total number of treatments in which extravasation occurred in the FOV (during live imaging) and in the five areas imaged after US exposure increased substantially.

The observed extravasation of NPs and dextran occurred at different time points and locations and occurred within milliseconds to minutes after the onset of US exposure (Fig. 4). The number of extravasation events was not particularly high immediately after administration of MBs when the concentration of MBs was highest. However, most of the extravasations occurred within the circulation half-life of the two MBs at higher MIs (3/3

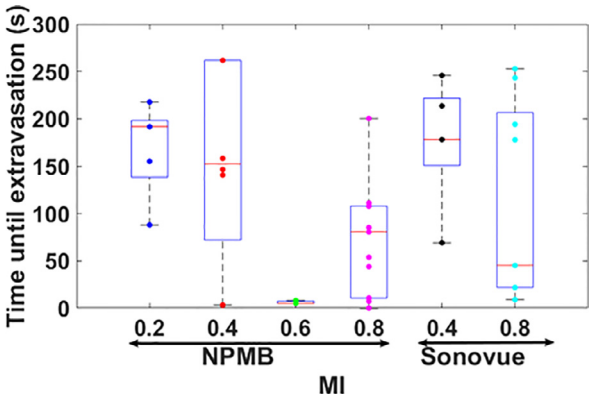

Fig. 4. Time point at which extravasation occurred after onset of US exposure. Both the data points and box-and-whisker plots are shown. Each point represents one blood vessel where extravasation was observed, and the *red line* in box-and-whisker plots represents the median. For NPMBs at MI = 0.2 (n = 5), MI = 0.4 (n = 8), MI = 0.6 (n=3) and MI = 0.8 (n = 17), and for Sonovue at MI = 0.4 (n=5) and MI = 0.8 (n=10) where n = number of blood vessels. Note: Because more than one extravasation could occur at the same time point in different vessels, two or more circles could be merged together. MI = mechanical index; NPMB = nanoparticle-stabilized microbubbles.

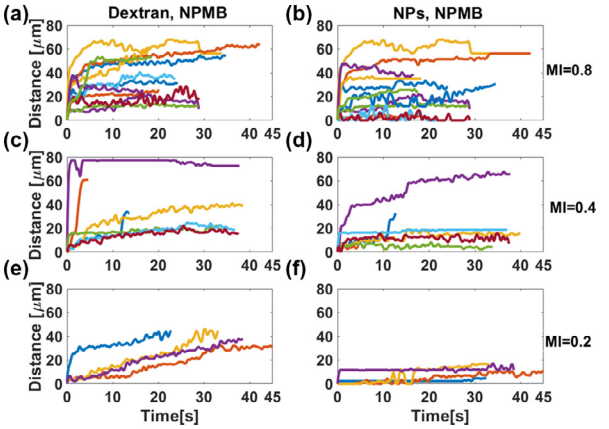

Fig. 5. Penetration of dextran and NPs for NPMBs at various MIs. MI = 0.8 for dextran (a) and NPs (b) (n = 12). MI = 0.4 for dextran (c) and NPs (d) (n = 7). MI = 0.2 for dextran (e) and NPs (f) (n = 4). Zero time corresponds to the time immediately before opening of the blood vessel by the ultrasound/MBs, and zero distance is inside the blood vessel where extravasation occurred. Each color represents one blood vessel in which extravasation occurred. MI = mechanical index; NPs = nanoparticles; NPMB = nanoparticle-stabilized microbubbles.

and 16/17 at MIs of 0.6 and 0.8, respectively, for NPMBs and 6/10 for Sonovue at an MI of 0.8).

A representative color map plot of mean fluorescence intensity as a function of both time after extravasation and distance from the blood vessel is provided in Supplementary Figure S4 (online only) for dextran (Supplementary Fig. S4a) and NPs (Supplementary Fig. S4b). Based on such color map plots, the intravascular intensity (Supplementary Figs. S5–S6) (online only), as well as the penetration and accumulation of NPs and dextran into the extravascular matrix (ROI in Supplementary Fig. S7) (online only), were determined (Figs. 5–8).

Interestingly, after extravasation, inside the blood vessels at the origin of extravasation, an immediate accumulation of dextran and NPs was observed followed by a slow decrease in dextran and NP fluorescence intensity. This effect occurred mainly at the higher MIs (0.8 and 0.4), whereas in some cases, for an MI of 0.2, dextran and NP fluorescence intensities inside blood vessels increased until the end of the treatment (Supplementary Figs. S5 and S6).

For both NPs and dextrans, there was a large variation in the extent of extravasation and subsequent penetration into the extracellular matrix between the individual extravasations, as illustrated in Figure 5 for NPMBs and in Figure 6 for Sonovue. The variation was more pronounced at MI = 0.8 for both MBs. Sonication at an MI of 0.8 induced more pronounced extravasation than sonication at the lower MIs, and in a few cases, it appeared immediately after a reduction or even full stop in blood flow, and change in blood flow direction occurred. The rate of penetration of both dextran and NPs into the extracellular matrix increased with increasing MI, as illustrated in Figures 5 and 6 for NPMBs and Sonovue, respectively. At an MI of 0.8 (for most cases), the penetration distance of the agents increased rapidly, as indicated by the steep initial slope (Figs. 5a, 5b and

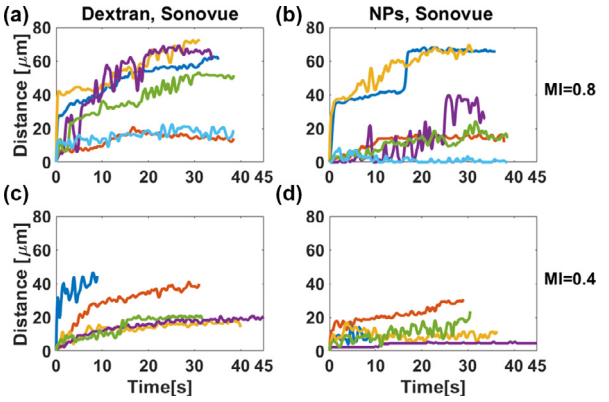

Fig. 6. Penetration of dextran and NPs for Sonovue at various MIs. MI = 0.8 for dextran (a) and NPs (b) (n = 6). MI = 0.4 for dextran (c) and NPs (d) (n = 5). Zero time corresponds to the time immediately before opening of the blood vessel by the ultrasound/MBs, and zero distance is inside the blood vessel where extravasation of agents occurred. Each color represents one blood vessel where extravasation occurred. MI = mechanical index; NPs = nanoparticles; NPMB = nanoparticle-stabilized microbubbles.

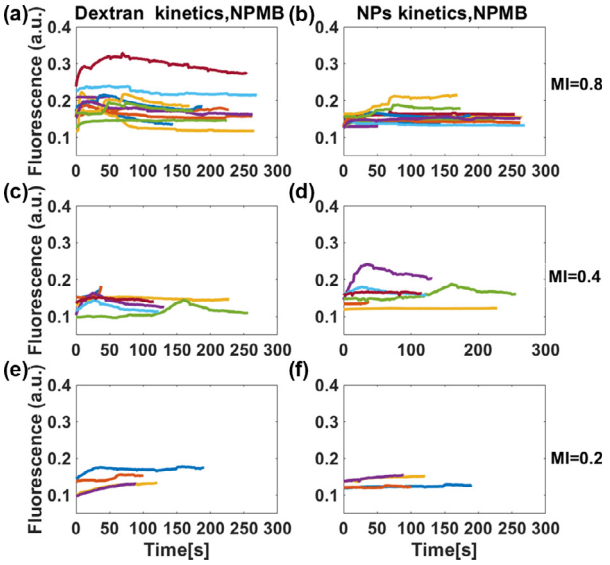

Fig. 7. Extravascular accumulation within 50 μm from the blood vessel of dextran and NPs as a function of time for NPMBs. MI = 0.8 for dextran (a) and NPs (b) (n = 12). MI = 0.4 for dextran (c) and NPs (d) (n = 7). MI = 0.2 for dextran (e) and NPs (f) (n = 4). Zero time corresponds to the time immediately before the extravasation. These curves are ratios to their respective maximum (whole image). Each color represents one blood vessel in which extravasation occurred. MI = mechanical index; NPs = nanoparticles; NPMB = nanoparticle-stabilized microbubbles.

6a, 6b). At the lower MIs (0.4 and 0.2) and at an MI of 0.4 using Sonovue, the rates of penetration of dextran and NPs were slower in most cases (Fig. 5c–f and 6c, 6d). When rapid and deep penetration into the extracellular matrix occurred (as illustrated by the *purple curve* in Figure 5c (MI = 0.4) and the *blue curve* in Figure 5e (MI = 0.2), a large aggregate of NPs or NPMBs was present intravascularly immediately before the onset of extravasation. Representative images for such large aggregates are provided in Supplementary Figure S8 (online only, for MI = 0.4) and Figure 3a (for MI = 0.2).

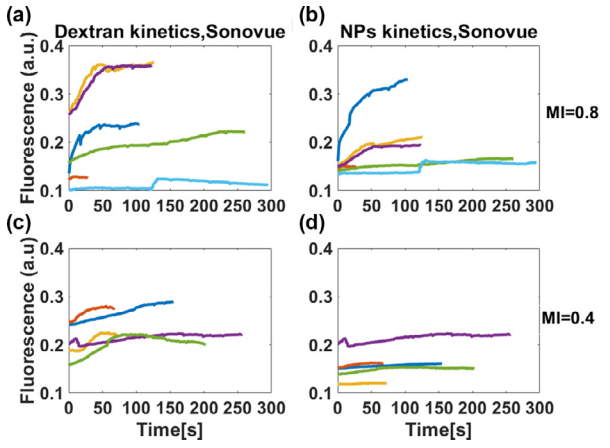

Fig. 8. Extravascular accumulation within 50 μm from the blood vessel of dextran and NPs as a function of time for Sonovue. MI = 0.8 for dextran (a) and NPs (b) (n = 6). MI = 0.4 for dextran (c) and NPs (d) (n = 5). Zero time corresponds to the time immediately before extravasation. These curves are ratios to their respective maximum (whole image). Each color represents one blood vessel where extravasation occurred. MI = mechanical index; NPs = nanoparticles; NPMB = nanoparticle-stabilized microbubbles.

The maximum penetration distances of the two agents within 40 s after the extravasation event varied considerably (Fig. 5 for NPMBs, Fig. 6 for Sonovue). At an MI of 0.8, the maximum penetration of dextran and NPs (in most of the extravasations) was in the ranges 38–70 and 23–70 μm, respectively, when NPMBs or Sonovue was injected (Figs. 5a, 5b and 6a, 6b).

At the lower MIs, when NPMBs were injected, the maximum penetration of dextran was in the ranges 34–77 and 38–46 μm at MIs of 0.4 and 0.2, respectively (Fig. 5c, 5e), while NPs penetrated in the ranges 16–77 μm at MI = 0.4 and 10–17 μm at MI = 0.2 (Fig. 5d, 5f). With Sonovue at MI = 0.4, the maximum penetration of dextran was in the range 31–46 μm, and for the NPs, it was in the range 17–30 μm (Fig. 6c, d).

Next, the accumulation of dextran and NPs within 50 μm of the blood vessel wall as a function of time was determined (Figs. 7 and 8) and exhibited a large variation between the individual extravasations. The extravascular mean fluorescence intensity increased with MI. For NPMBs at MIs of 0.8 and 0.4, the mean fluorescence intensity for dextran (for most extravasations) increased immediately after the onset of the extravasation and reached a peak before a gradual decrease in intensity was observed, whereas the NP fluorescence intensity increased more slowly in the beginning and leveled out thereafter (Fig. 7a, 7b). At an MI of 0.2, the increase in the mean intensity of both dextran and NPs was low (Fig. 7e, 7f). For Sonovue at MI = 0.8, both dextran and NPs exhibited a gradual increase in fluorescence intensity (in most cases) followed by a slow increase (Fig. 8a, 8b), whereas the increase was much less at MI = 0.4 (Fig. 8a, 8b and 7c, 7d).

Blood vessel diameter, branching point and extravasation

The vessel diameter was important for extravasation. At lower MIs (0.2–0.4), extravasation of NPs and dextran occurred in vessels with larger diameters as compared with that at MIs of 0.8 and 0.6 (Fig. 9a). Statistical analysis revealed significant differences between MIs of 0.8 and 0.2 and between MIs of 0.8 and 0.4 (Fig. 9a). Furthermore, for all MIs tested, 80% of the extravasation of NPs and dextran occurred at the vessel branching points, as outlined in Table 2, Figure 9b and Supplementary Videos S1 and S3 (online only). "At

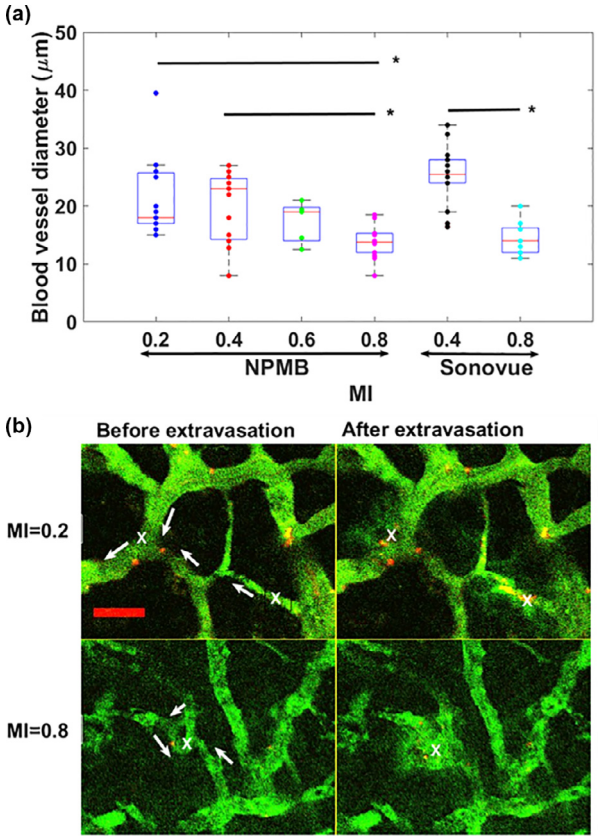

Fig. 9. (a) Blood vessel diameter versus MI. Both the data points and box-and-whisker plot are shown. Each circle represents one blood vessel in which extravasation was observed, and the *red line* in the box-and-whisker plot represents the median. For NPMBs at MI = 0.2 (n = 15), MI = 0.4 (n = 16), MI = 0.6 (n = 5) and MI = 0.8 (n = 17) and for Sonovue at MI = 0.4 (n = 15) and MI = 0.8 (n = 11). n is number of blood vessels. *Statistically significant difference between the groups. B) Examples of positions where extravasation occurred. *Arrows* indicate the flow direction, × indicates the position where extravasation occurred for MI = 0.2 (NPMBs) and MI = 0.8 (NPMBs). Bar = 50 μm. MI = mechanical index; NPs = nanoparticles; NPMB = nanoparticle-stabilized microbubbles.

vessel branching points" means a maximum of 9 μm from the vessel wall plus the radius of the vessel.

Change in blood flow caused by US and MBs

Before injection of MBs and application of US, a homogeneous FITC−dextran fluorescence signal was observed (Fig. 10a). During US exposure, many vessels exhibited heterogeneous and more granular FITC−dextran fluorescence signals (Fig. 10b). This appearance was more pronounced when the blood flow stopped and/or changed direction (Supplementary Video S3). We did not observe such effects in the control groups (without US) (Supplementary Videos S6 and S7). A reduction in mean fluorescence intensity inside the blood vessel was observed immediately when US was applied. This reduction increased with increasing MI and might be due to a slight change of focus of imaging caused by displacement of the tissue by acoustic radiation force.

The speed of NPs in untreated and US-treated tumors is illustrated in Figure 10c. Before application of US (controls), after injection of NPMBs, the speed was 117 ± 40 μm/s. When free NPs and Sonovue were injected, the speed was significantly lower, that is, 91 ± 30 μm/s. After US, the speed of NPs decreased by approximately 41%, 63% and 89% at MIs of 0.2, 0.4 and 0.8, respectively, for the NPMB groups, and by approximately 70% for both Sonovue groups. The difference between NP speed before US and that during US was statistically significant at all MIs and for both MBs. Moreover, statistical analysis revealed significant differences between all NPMB groups, but no significant difference between MIs of 0.4 and 0.8 for Sonovue groups.

Moreover, US combined with MBs altered the blood flow direction, as illustrated in Figure 10d and Supplementary Video S3. The percentage of occurrence of changes in blood flow direction for each group increased with MI (Fig. 10d). At the highest MI, approximately 50% of the recordings revealed a change in the flow direction. We did not observe any change in flow direction for the groups injected with Sonovue only and Sonovue plus free NPs without US.

Blood vessel damage caused by US and MBs

Histologic HES-stained sections were imaged and evaluated for US-induced damage by an experienced pathologist. In Figure 11 are representative images of tumors treated with Sonovue at an MI of 0.4 (Fig. 11a) and NPMBs at an MI of 0.8 (Fig. 11b). Microhemorrhages (extravasation of red blood cells out of the blood vessel) were observed at MI = 0.8 (Fig. 11c) in 2 of 5 mice in the NPMB group and 1 of 4 mice in the Sonovue group. No

Table 2. Numbers of extravasations that occurred at branching point of a blood vessel

	NPMBs				Sonovue		Total
	MI = 0.2	MI = 0.4	MI = 0.6	MI = 0.8	MI = 0.4	MI = 0.8	
At branching point	3	7	2	13	4	9	38
Not close to branching point	2	1	1	4	1	1	10

MI = mechanical index; NPMB = in-house-made microbubbles stabilized by polymeric nanoparticles.

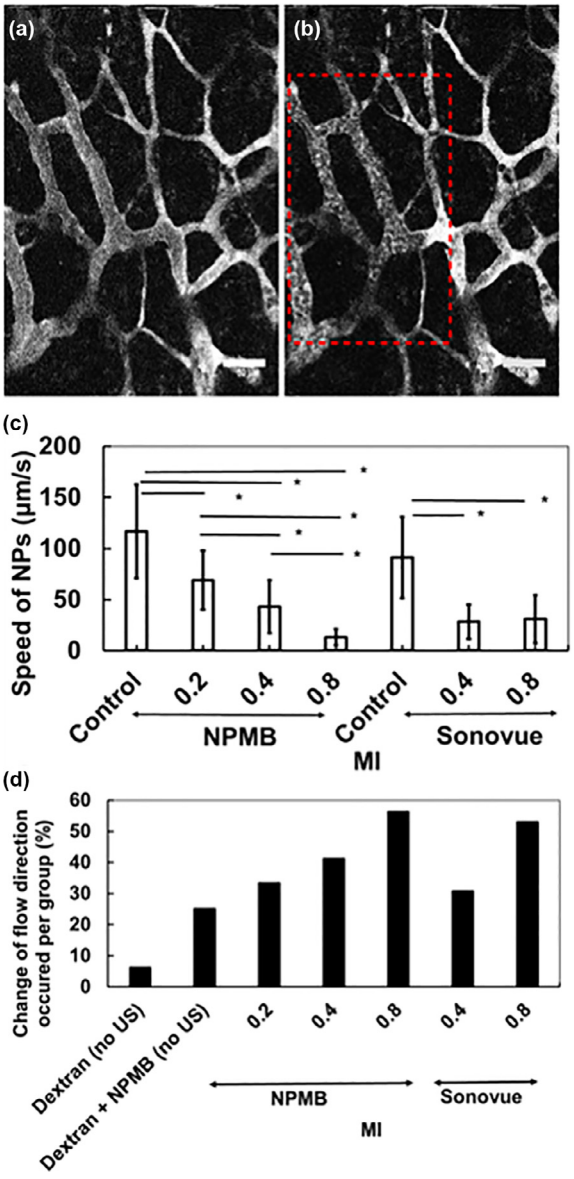

Fig. 10. Change in blood flow and speed of NPs. Representative image of homogenous fluorescein isothiocyanate–dextran signal intensity before (a) and after (b) US exposure. Change in blood flow rate and direction during US exposure (17.4 s after NPMB injection and US exposure). (c) Speed of the NPs as function of MI for control (no US) and during US for both NPMBs and Sonovue. (d) Percentage occurrence of change in blood flow direction observed per total recordings versus MI for both MBs. Results (c) are from four mice for NPMB control and three mice each for the other groups; error bars are for total number of particles analyzed. Results (d) are for n = 16 for dextran (no US), n = 4 for dextran + NPMB-US, n = 3 each for Sonovue (no US) and Sonovue + NPs, where n is number of animals. See Table 1 for NPMB + US and Sonovue + US groups for number of treatments in each group. *Statistically significant difference between the groups. Bar = 50 μm. MI = mechanical index; NPs = nanoparticles; NPMB = nanoparticle-stabilized microbubbles; US = ultrasound.

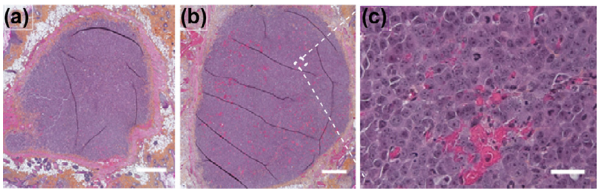

Fig. 11. Representative histologic sections from the OHS tumors grown in dorsal window chambers treated with MB and US stained with hematoxylin, erythrosine and saffron. (a) Treated at MI = 0.4. (b) Treated at MI = 0.8. (c) Higher-magnification image from the *white box* in (b). Images were taken at 10 × (a, b) and 40 × (c) magnification. Bar = 1 mm (a, b) and 50 μm (c).

severe vascular damage was observed *per se*. No hemorrhages were observed at the lower MIs (0 of 4 mice each at MI = 0.4 for NPMB and Sonovue groups, and 0 of 2 mice each at MI = 0.2 for NPMB and Sonovue groups).

DISCUSSION

Real-time imaging of US-induced effects on the vasculature and behavior of various molecules and nanoscale particles is a powerful method. Multiphoton imaging of the opening of the blood–brain barrier has previously been performed (Burgess et al. 2014; Cho et al. 2011; Raymond et al. 2007). However, to our knowledge, real-time imaging of US-induced extravasation of nanoscale agents in solid tumors *in vivo* has not been reported before. In our study, imaging the vasculature by intravital multiphoton microscopy during US sonication revealed extravasation of NPs and dextran, which indicates opening of the blood vessel. There was a correlation between blood vessel size where extravasation occurred and MI. Furthermore, the majority of the extravasations occurred at vessel branching points. Moreover, US-induced changes in flow rate and flow direction were observed, and occasionally, the blood flow stopped for short periods.

One interesting observation is that in most cases where extravasation occurred, it occurred close to vessel branching points. This could partly be due to the chaotic and disorganized tumor vessels, which had trifurcations and branches with uneven diameters (Fukumura and Jain 2007), and the fragility of the branching points. It has been reported that the organization of the vessels can create differences in sensitivity to sonication (Hu et al. 2012) and that branching points of the tumor vessels could be more susceptible to sonication. It was also reported that microdisruption occurred more often at branching points, which could be due to MBs being more easily trapped at such locations (Raymond et al. 2007). Moreover, the blood flow pattern is different at

the branching point (Malek et al. 1999). The flow might influence the number of bubbles in contact with endothelial cells and the average bubble−cell distance, which can enhance the interaction between the bubbles and endothelial cells.

The diameter of the blood vessel was also found to affect US-induced extravasation. After sonication at higher MIs (0.8 and 0.6), extravasation was typically observed in vessels with diameters of approximately 10−20 μm, whereas at lower MIs (0.2 and 0.4), the diameter ranged from 20−40 μm. Such a correlation between MI and vessel diameter has been reported in other studies (Nhan et al. 2013; Raymond et al. 2007). The boundary conditions imposed by the vessel wall influence the resonance frequency and the oscillation of a MB (Goertz 2015; Qin and Ferrara 2007; Sassaroli and Hynynen 2005). If the effect is a reduction in bubble resonance frequency compared with a free space situation and the bubble resonance frequency falls below the sonication frequency in the smallest vessels (diameter 10−20 μm), a higher MI will typically be required to obtain the same effect from cavitation. This requirement might explain why we did not observe extravasation in the smallest vessels, except at the highest MI.

Another interesting observation is that the extravasations appeared within milliseconds to minutes after the onset of US exposure, which indicates that the MBs could be present in the circulation for 5 min. However, we did not observe a higher number of extravasations immediately after the bolus injection when the MB concentration was highest. The differences in tumor characteristics, such as blood vessel density, branching, vessel organization and blood flow velocity (Wilhelm et al. 2016), can cause fluctuations in the amount of MBs in the target region, thereby affecting the onset time of the extravasation (Choi et al. 2014). Furthermore, there may not be adequate time for reperfusion between US pulses after the US destruction of the MBs, which occurs in a considerably larger region than the FOV.

Sonication at MI = 0.8 induced more violent extravasation and a higher number of extravasation events than that at lower MI. The main mechanism for this violent extravasation could be inertial cavitation, which occurs at higher peak negative pressures, as bubbles respond with a large and unstable expansion and, finally, a violent collapse (Kooiman et al. 2014). The opening of the blood vessel wall is most likely due to mechanical forces induced on the vessel wall during the oscillation of the MBs and subsequent collapse, causing shear forces and secondary effects, such as microstreaming, shock waves and jetting. At the lower MIs (0.4 and 0.2), in most cases, slower extravasation was observed. At lower MIs, stable volumetric oscillation of MBs might induce mechanical forces and acoustic streaming, resulting in shear stress on the vessel wall that can be sustained during the entire pulse duration (Kooiman et al. 2014). These mechanisms can create pores in the vessel wall, causing material to extravasate from the vessel. Larger shear stresses are reported to create larger pore sizes or more prolonged pore openings (Helfield et al. 2016). For monodisperse MBs, in the healthy vasculature of the brain, the opening volume is proportional to the acoustic pressure (Vlachos et al. 2011). This finding indicates that the shear stress may be larger at higher MIs than at lower MIs, and larger openings are probably created.

A large variation in penetration and accumulation into the extracellular matrix between individual extravasations was observed for both MBs and at all MIs applied. The reason might be owing mainly to the following factors: 1) The size differences in the pores created on the blood vessel wall caused by polydisperse MBs exerting different shear stresses on the blood vessel wall: The diameter of monodisperse MBs has been reported to correlate with the volume of blood−brain barrier opening in the healthy vasculature of the brain (Vlachos et al. 2011). In our study, both MBs are polydisperse populations, and for the NPMB, the excess of free NPs or the NPMBs can aggregate, increasing the polydispersity. 2) Blood flow velocity variability within and between tumors: This variation will not only affect the amount of MBs within the target region but also the amount of NPs (and, to a lesser extent, dextran) within the target region. In some cases, arrival of few NPs was observed in the region in which extravasation was observed. 3) Properties of the extracellular matrix, such as the heterogeneity in tumor cell density, interstitial fluid pressure and stromal content, might also influence the penetration of the agents.

A PRF of 0.5 Hz was initially chosen based on the velocity of blood in capillaries of mice, which is 2.03 ±1.42 mm/s (Unekawa et al. 2010), and our previous *in vivo* study (Snipstad et al. 2017). However, reducing the PRF from 0.5 to 0.1 Hz caused an increase in the number of extravasations at an MI of 0.8 when Sonovue was used and an MI of 0.4 when NPMBs were injected. With the higher PRF, MBs could possibly be destroyed before they reach the FOV, as the size of the −3-dB US beam is considerably larger than the FOV. Hence, new MBs would not replace the destroyed MBs, and subsequent US pulses would be ineffective. With a PRF of 0.1 Hz, the MBs get more time to replace the destroyed MBs before the next US pulse arrives, hence improving the interaction between US and MBs in the FOV.

The total numbers of extravasation events induced by the two MBs differed. It has been reported that the type of MB has a significant effect on cavitation activity (McMahon and Hynynen 2017; Wang et al. 2014a). When US and Sonovue are combined, considerably

fewer extravasations and numbers of blood vessels affected were observed in the FOV (during live imaging) compared with what was observed when US and NPMBs were combined. The difference in inducing extravasation is probably due to differences in the properties and behavior of the two MBs. The average diameter and concentration injected are quite similar for the two MBs. The size distributions of the two MBs are rather similar; however, the NPMBs are a small population with a diameter larger than 10 μm. In addition, the circulation half-time of the NPMBs is 1.5−2 times longer than that of Sonovue; hence, the amount of MBs reaching the tumor tissue could be different. The shell and gas core of the two MBs differ. NPMBs have an NP/protein shell and perfluoropropane core, whereas Sonovue has a lipid shell and sulfur hexafluoride (SF_6) core. The NP/protein shell is thicker and stiffer compared with the lipid shell, which is soft and elastic. The shell composition is important to the behavior of the MBs, and its importance was described in a study comparing Optison with a shell of denatured albumin and lipid-shelled Definity, where Optison induced greater destruction of the blood−brain barrier than Definity (McDannold et al. 2007). These researchers also suggest that the lipid-shelled Definity may be more difficult to break than Optison. However, our findings suggest that NPs/protein-shelled NPMBs may be more difficult to break than the lipid-shelled Sonovue and thus resilient at higher MIs. Therefore, the cavitation activity can persist longer for NPMBs than for Sonovue, causing more microstreaming and microjets affecting the capillary walls.

At an MI of 0.8, penetration of NPs into the extracellular matrix was faster for NPMBs than for Sonovue. This could be due to the presence of NPs on the bubble shell for the NPMBs which, upon violent destruction of MBs, are spread more efficiently than circulating particles (Burke et al. 2011a, 2014). Dextran penetrated faster than NPs for both MBs and at all MIs applied. The difference in the rate of penetration between NPs and dextran could be due to their sizes. The diameter of the NPs is approximately 160 nm, whereas the diameter of 2-MDa dextran is reported to be approximately 60 nm (Lammers et al. 2015). Moreover, the extravascular mean fluorescence intensity of dextran and NPs increases with MI, reflecting the correlation between MI and amount of NPs and dextrans extravasating.

Changes in blood flow rate and direction were also assessed from real-time imaging. Interestingly, changes in flow rate and direction were observed at all MIs applied, but the changes in both flow rate and direction were more pronounced at higher MI (0.8). As previously reported (Raymond et al. 2007), we observed heterogeneous and a granulation or streak of the FITC−dextran fluorescence in many vessels when the blood flow stopped and/or changed flow direction during US exposure. The black structures within the vessels in the heterogeneous FITC−dextran fluorescence could be red blood cells and became more apparent when the flow rate decreased. No changes in blood flow direction were observed during the 5 min of imaging after injection of Sonovue or Sonovue plus NPs before exposure to US. However, without US, the NP flow speed was significantly lower when injecting Sonovue plus free NPs than NPMBs (91 ± 30 μm/s vs. 117 ± 40 μm/s). However, the mechanisms responsible for change of flow during US are not fully understood. A reduction of blood velocity and perfusion caused by US combined with MBs (at 1-MHz peak negative pressure in the range 0.74−1.6 MPa) was also reported in previous studies (Burke et al. 2011b; Goertz et al. 2008, 2012). In these studies, the effects are associated with inertial cavitation (Goertz 2015). In our study, the change in blood flow was also found at an MI of 0.2, where inertial cavitation can be ruled out. This indicates that other mechanisms are involved. For example, (i) aggregation and activation of platelets can apparently occur very rapidly after an injury to the endothelial cells because of rapid destruction of MBs at the surface of tumor vasculature, which reduces the blood flow (Hu et al. 2012); and (ii) there might be significant cavitation activity going on in nearby arterioles outside the FOV that potentially can induce vasoconstriction and affect the flow within the FOV. The occurrence of vasoconstriction has been reported to induce a reduction and transiently stop blood flow (Raymond et al. 2007).

From histologic evaluation, the tissue was not damaged at MIs of 0.4 and 0.2, as also reported in our previous study (Snipstad et al. 2017). At an MI of 0.8, microhemorrhage was observed in the tumor tissue and was considered to be minimal. Similar effects have been reported previously for Sonovue at an MI of 0.8 (Wu et al. 2017). The microhemorrhages could be caused by the fragile neoangiogenic vessels of the tumors.

CONCLUSIONS

Multiphoton microscopy was used for real-time intravital imaging during US to investigate the effects of US and MBs in enhancing the permeability of tumor blood vessels and improving the delivery of NPs. Large variations in the rate and extent of penetration into the extracellular matrix were observed. Interestingly, at the higher MI, the extravasation occurred in smaller vessels and extravasation generally occurred close to vessel branching points. US also altered NP flow velocity and blood flow direction in an MI-dependent manner.

Results gained from intravital multiphoton microscopy help to elucidate the temporal and spatial extravasation of nanoscale particles during US exposure, which is highly useful in understanding the mechanisms underlying US-mediated delivery of NPs and optimizing them.

Acknowledgments—The authors are grateful to Spiros Kotopoulis for his assistance in designing the transducer cone, Anne Rein Hatletveit (SINTEF) for producing NPs and NPMBs and Annemieke Van Wamel for assisting in handling the animals. The project is supported by The Research Council of Norway (Project No. 240316). Additional funding from the Central Norway Regional Health Authority is much appreciated. Housing and care of animals were provided by the Comparative Medicine Core Facility (CoMed), and sectioning and HES staining were provided by the Cellular and Molecular Imaging Core Facility (CMIC), both at Norwegian University of Science and Technology (NTNU), funded by the Faculty of Medicine and Health Sciences at NTNU and Central Norway Regional Health Authority.

Conflict of interest disclosure—The authors declare no competing interests.

SUPPLEMENTARY DATA

Supplementary data related to this article can be found online at doi:10.1016/j.ultrasmedbio.2019.07.683.

REFERENCES

Anchordoquy TJ, Barenholz Y, Boraschi D, Chorny M, Decuzzi P, Dobrovolskaia MA, Farhangrazi ZS, Farrell D, Gabizon A, Ghandehari H, Godin B, La-Beck NM, Ljubimova J, Moghimi SM, Pagliaro L, Park JH, Peer D, Ruoslahti E, Serkova NJ, Simberg D. Mechanisms and barriers in cancer nanomedicine: Addressing challenges, looking for solutions. ACS Nano 2017;11:12–18.

Antonios NP, James JC. Superharmonic microbubble Doppler effect in ultrasound therapy. Phys Med Biol 2016;61:6154.

Åslund AKO, Berg S, Hak S, Mørch Ý, Torp SH, Sandvig A, Widerøe M, Hansen R, Davies CDL. Nanoparticle delivery to the brain—By focused ultrasound and self-assembled nanoparticle-stabilized microbubbles. J Control Release 2015;220:287–294.

Boissenot T, Bordat A, Fattal E, Tsapis N. Ultrasound-triggered drug delivery for cancer treatment using drug delivery systems: From theoretical considerations to practical applications. J Control Release 2016;241:144–163.

Burgess A, Nhan T, Moffatt C, Klibanov AL, Hynynen K. Analysis of focused ultrasound-induced blood–brain barrier permeability in a mouse model of Alzheimer's disease using two-photon microscopy. J Control Release 2014;192:243–248.

Burke CW, Hsiang YHJ, Alexander IVE, Kilbanov AL, Price RJ. Covalently Linking poly(lactic-co-glycolic acid) nanoparticles to microbubbles before intravenous injection improves their ultrasound-targeted delivery to skeletal muscle. Small 2011a;7:1227–1235.

Burke CW, Klibanov AL, Sheehan JP, Price RJ. Inhibition of glioma growth by microbubble activation in a subcutaneous model using low duty cycle ultrasound without significant heating. J Neurosurg 2011b;114:1654–1661.

Burke CW, Alexander E, Timbie K, Kilbanov AL, Price RJ. Ultrasound-activated agents comprised of 5 FU-bearing nanoparticles bonded to microbubbles inhibit solid tumor growth and improve survival. Mol Ther 2014;22:321–328.

Carpentier A, Canney M, Vignot A, Reina V, Beccaria K, Horodyckid C, Karachi C, Leclercq D, Lafon C, Chapelon JY, Capelle L, Cornu P, Sanson M, Hoang-Xuan K, Delattre JY, Idbaih A. Clinical trial of blood–brain barrier disruption by pulsed ultrasound. Sci Transl Med 2016;8:343. re2.

Caskey CF, Stieger SM, Qin S, Dayton PA, Ferrara KW. Direct observations of ultrasound microbubble contrast agent interaction with the microvessel wall. J Acoust Soc Am 2007;122:1191–1200.

Chen H, Brayman AA, Bailey MR, Matula TJ. Blood vessel rupture by cavitation. Urol Res 2010;38:321–326.

Chen H, Kreider W, Brayman AA, Bailey MR, Matula TJ. Blood vessel deformations on microsecond time scales by ultrasonic cavitation. Phys Rev Lett 2011;106 034301.

Cho EE, Drazic J, Ganguly M, Stefanovic B, Hynynen K. Two-photon fluorescence microscopy study of cerebrovascular dynamics in ultrasound-induced blood–brain barrier opening. J Cereb Blood Flow Metab 2011;31:1852–1862.

Choi JJ, Carlisle RC, Coviello C, Seymour L, Coussios CC. Non-invasive and real-time passive acoustic mapping of ultrasound-mediated drug delivery. Phys Med Biol 2014;59:4861–4877.

Coates A, Abraham S, Kaye SB, Sowerbutts T, Frewin C, Fox RM, Tattersall MHN. On the receiving end—Patient perception of the side-effects of cancer chemotherapy. Eur J Cancer Clin Oncol 1983;19:203–208.

Dayton P, Klibanov A, Brandenburger G, Ferrara K. Acoustic radiation force in vivo: A mechanism to assist targeting of microbubbles. Ultrasound Med Biol 1999;25:1195–1201.

Dimcevski G, Kotopoulis S, Bjånes T, Hoem D, Schjøtt J, Gjertsen BT, Biermann M, Molven A, Sorbye H, McCormack E, Postema M, Gilja OH. A human clinical trial using ultrasound and microbubbles to enhance gemcitabine treatment of inoperable pancreatic cancer. J Control Rel 2016;243:172–181.

Eggen S, Fagerland SM, Mørch Ý, Hansen R, Søvik K, Berg S, Furu H, Bøhn AD, Lilledahl MB, Angelsen A, Angelsen B, Davies CDL. Ultrasound-enhanced drug delivery in prostate cancer xenografts by nanoparticles stabilizing microbubbles. J Control Rel 2014;187:39–49.

Fodstad Ø, Brøgger A, Bruland Ø, Solheim OP, Nesland JM, Pihl A. Characteristics of a cell line established from a patient with multiple osteosarcoma, appearing 13 years after treatment for bilateral retinoblastoma. Int J Cancer 1986;38:33–40.

Fukumura D, Jain RK. Tumor microenvironment abnormalities: Causes, consequences, and strategies to normalize. J Cell Biochem 2007;101:937–949.

Garbin V, Cojoc D, Ferrari E, Di Fabrizio E, Overvelde MLJ, van der Meer SM, de Jong N, Lohse D, Versluis M. Changes in microbubble dynamics near a boundary revealed by combined optical micromanipulation and high-speed imaging. Appl Phys Lett 2007;90 114103.

Goertz DE. An overview of the influence of therapeutic ultrasound exposures on the vasculature: High intensity ultrasound and microbubble-mediated bioeffects. Int J Hyperthermia 2015;31:134–144.

Goertz DE, Karshafian R, Hynynen K. Antivascular effects of pulsed low intensity ultrasound and microbubbles in mouse tumors. Proc IEEE Int Ultrason Symp 2008;670–673.

Goertz DE, Todorova M, Mortazavi O, Agache V, Chen B, Karshafian R, Hynynen K. Antitumor effects of combining docetaxel (Taxotere) with the antivascular action of ultrasound stimulated microbubbles. PLoS One 2012;7:e52307.

Hak S, Reitan NK, Haraldseth O, Davies CDL. Intravital microscopy in window chambers: A unique tool to study tumor angiogenesis and delivery of nanoparticles. Angiogenesis 2010;13:113–130.

Helfield BL, Leung BYC, Goertz DE. The effect of boundary proximity on the response of individual ultrasound contrast agent microbubbles. Phys Med Biol 2014;59:1721–1745.

Helfield B, Chen X, Watkins SC, Villanueva FS. Biophysical insight into mechanisms of sonoporation. Proc Natl Acad Sci USA 2016;113:9983.

Hernot S, Klibanov AL. Microbubbles in ultrasound-triggered drug and gene delivery. Adv Drug Deliv Rev 2008;60:1153–1166.

Hu X, Kheirolomoom A, Mahakian LM, Beegle JR, Kruse DE, Lam KS, Ferrara KW. Insonation of targeted microbubbles produces regions of reduced blood flow within tumor vasculature. Invest Radiol 2012;47:398–405.

Hynynen K, McDannold N, Vykhodtseva N, Jolesz FA. Noninvasive MR imaging–guided focal opening of the blood–brain barrier in rabbits. Radiology 2001;220:640–646.

Klymchenko AS, Roger E, Anton N, Anton H, Shulov I, Vermot J, Mely Y, Vandamme TF. Highly lipophilic fluorescent dyes in nano-emulsions: Towards bright non-leaking nano-droplets. RSC Adv 2012;2:11876–11886.

Kooiman K, Vos HJ, Versluis M, de Jong N. Acoustic behavior of microbubbles and implications for drug delivery. Adv Drug Deliv Rev 2014;72:28–48.

Kotopoulis S, Delalande A, Popa M, Mamaeva V, Dimcevski G, Gilja OH, Postema M, Gjertsen BT, McCormack E. Sonoporation-enhanced chemotherapy significantly reduces primary tumour burden in an orthotopic pancreatic cancer xenograft. Mol Imaging Biol 2014;16:53–62.

Lammers T, Kiessling F, Hennink WE, Storm G. Drug targeting to tumors: Principles, pitfalls and (pre-) clinical progress. J Control Release 2012;161:175–187.

Lammers T, Koczera P, Fokong S, Gremse F, Ehling J, Vogt M, Pich A, Storm G, van Zandvoort M, Kiessling F. Theranostic USPIO-loaded microbubbles for mediating and monitoring blood–brain barrier permeation. Adv Funct Mater 2015;25:36–43.

Lammertink B, Bos C, Deckers R, Storm G, Moonen C, Escoffre JM. Sonochemotherapy: From bench to bedside. Front Pharmacol 2015;6:138.

Liu HL, Hua MY, Chen P-Y, Chu PC, Pan CH, Yang HW, Huang CY, Wang JJ, Yen TC, Wei KC. Blood–brain barrier disruption with focused ultrasound enhances delivery of chemotherapeutic drugs for glioblastoma treatment. Radiology 2010;255:415–425.

Maeda H, Wu J, Sawa T, Matsumura Y, Hori K. Tumor vascular permeability and the EPR effect in macromolecular therapeutics: A review. J Control Rel 2000;65:271–284.

Mainprize T, Lipsman N, Huang Y, Meng Y, Bethune A, Ironside S, Heyn C, Alkins R, Trudeau M, Sahgal A, Perry J, Hynynen K. Blood–brain barrier opening in primary brain tumors with non-invasive MR-guided focused ultrasound: A clinical safety and feasibility study. Sci Rep 2019;9:321.

Malek AM, Alper SL, Izumo S. Hemodynamic shear stress and its role in atherosclerosis. JAMA 1999;282:2035–2042.

McDannold N, Vykhodtseva N, Hynynen K. Use of ultrasound pulses combined with Definity for targeted blood–brain barrier disruption: A feasibility study. Ultrasound Med Biol 2007;33:584–590.

McMahon D, Hynynen K. Acute inflammatory response following increased blood–brain barrier permeability induced by focused ultrasound is dependent on microbubble dose. Theranostics 2017;7:3989–4000.

Mullick Chowdhury S, Lee T, Willmann JK. Ultrasound-guided drug delivery in cancer. Ultrasonography 2017;36:171–184.

Mørch Ý, Hansen R, Berg S, Aslund AKO, Glomm WR, Eggen S, Schmid R, Johnsen H, Kubowicz S, Snipstad S, Sulheim E, Hak S, Singh G, McDonagh BH, Blom H, Davies CDL, Stenstad PM. Nanoparticle-stabilized microbubbles for multimodal imaging and drug delivery. Contrast Media Mol Imaging 2015;10:356–366.

Nhan T, Burgess A, Cho EE, Stefanovic B, Lilge L, Hynynen K. Drug delivery to the brain by focused ultrasound induced blood–brain barrier disruption: Quantitative evaluation of enhanced permeability of cerebral vasculature using two-photon microscopy. J Control Release 2013;172:274–280.

Qin S, Ferrara KW. The natural frequency of nonlinear oscillation of ultrasound contrast agents in microvessels. Ultrasound Med Biol 2007;33:1140–1148.

Raymond SB, Skoch J, Hynynen K, Bacskai BJ. Multiphoton imaging of ultrasound/Optison mediated cerebrovascular effects in vivo. J Cereb Blood Flow Metab 2007;27:393–403.

Sassaroli E, Hynynen K. Resonance frequency of microbubbles in small blood vessels: A numerical study. Phys Med Biol 2005;50:5293–5305.

Schneider M. Characteristics of SonoVue™. Echocardiography 1999;16:743–746.

Snipstad S, Berg S, Mørch Ý, Bjørkøy A, Sulheim E, Hansen R, Grimstad I, van Wamel A, Maaland AF, Torp SH, Davies CDL. Ultrasound improves the delivery and therapeutic effect of nanoparticle-stabilized microbubbles in breast cancer xenografts. Ultrasound Med Biol 2017;43:2651–2669.

Sulheim E, Kim J, van Wamel A, Kim E, Snipstad S, Vidic I, Grimstad IH, Widerøe M, Torp SH, Lundgren S, Waxman DJ, Davies CDL. Multi-modal characterization of vasculature and nanoparticle accumulation in five tumor xenograft models. J Control Release 2018;279:292–305.

Tannock IF, Lee CM, Tunggal JK, Cowan DSM, Egorin MJ. Limited penetration of anticancer drugs through tumor tissue. Clin Cancer Res 2002;8:878.

Treat LH, McDannold N, Zhang Y, Vykhodtseva N, Hynynen K. Improved anti-tumor effect of liposomal doxorubicin after targeted blood–brain barrier disruption by MRI-guided focused ultrasound in rat glioma. Ultrasound Med Biol 2012;38:1716–1725.

Unekawa M, Tomita M, Tomita Y, Toriumi H, Miyaki K, Suzuki N. RBC velocities in single capillaries of mouse and rat brains are the same, despite 10-fold difference in body size. Brain Res 2010;1320:69–73.

van Wamel A, Sontum PC, Healey A, Kvåle S, Bush N, Bamber J, de Lange Davies C. Acoustic Cluster Therapy (ACT) enhances the therapeutic efficacy of paclitaxel and Abraxane for treatment of human prostate adenocarcinoma in mice. J Control Rel 2016;236:15–21.

Vlachos F, Tung YS, Konofagou E. Permeability dependence study of the focused ultrasound-induced blood–brain barrier opening at distinct pressures and microbubble diameters using DCE-MRI. Magn Reson Med 2011;66:821–830.

Wang S, Samiotaki G, Olumolade O, Feshitan JA, Konofagou EE. Microbubble type and distribution dependence of focused ultrasound-induced blood–brain barrier opening. Ultrasound Med Biol 2014a;40:130–137.

Wang TY, Wilson KE, Machtaler S, Willmann JK. Ultrasound and microbubble guided drug delivery: Mechanistic understanding and clinical implications. Curr Pharm Biotechnol 2014b;14:743–752.

Wang TY, Choe JW, Pu K, Devulapally R, Bachawal S, Machtaler S, Chowdhury SM, Luong R, Tian L, Khuri-Yakub B, Rao J, Paulmurugan R, Willmann JK. Ultrasound-guided delivery of microRNA loaded nanoparticles into cancer. J Control Release 2015;203:99–108.

Wei KC, Chu PC, Wang HYJ, Huang CY, Chen PY, Tsai HC, Lu YJ, Lee PY, Tseng IC, Feng LY, Hsu PW, Yen TC, Liu HL. Focused ultrasound-induced blood–brain barrier opening to enhance temozolomide delivery for glioblastoma treatment: A preclinical study. PLoS One 2013;8:e58995.

Wilhelm S, Tavares AJ, Dai Q, Ohta S, Audet J, Dvorak HF, Chan WC. Analysis of nanoparticle delivery to tumours. Nat Rev Mater 2016;1:16014.

Wu SK, Chu PC, Chai WY, Kang ST, Tsai CH, Fan CH, Yeh CK, Liu HL. Characterization of different microbubbles in assisting focused ultrasound-induced blood–brain barrier opening. Sci Rep 2017;7:46689.